

# JOURNAL OF THE AMERICAN CHEMICAL SOCIETY

Registered in U.S. Patent Office. © Copyright, 1975, by the American Chemical Society

VOLUME 97, NUMBER 20

OCTOBER 1, 1975

## A Qualitative Molecular Orbital Picture of Electronegativity Effects on $\text{XH}_3$ Inversion Barriers

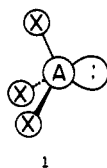
Charles C. Levin

Contribution from the Department of Chemistry, Smith College,  
Northampton, Massachusetts 01060. Received December 28, 1974

**Abstract:** A Walsh-type molecular orbital picture of central atom electronegativity effects on  $\text{XH}_3$  inversion barriers is presented. The large barrier increase with decreasing electronegativity is linked to a parallel decrease in HOMO-LUMO splitting in the  $D_{3h}$  transition state. The relationship of this splitting to level spacings in the corresponding united atoms as well as to the second-order Jahn-Teller effect of Bader and Pearson is discussed. Substituent effects are briefly considered.

Pyramidal inversion of trivalent group 5 derivatives and their group 4 and 6 analogs has been a topic of intense experimental and theoretical interest<sup>1-7</sup> ever since the detection of inversion doubling by Dennison and Uhlenbeck in 1932.<sup>8</sup> One of the most intriguing aspects of the inversion process is its sensitivity to the nature of the group 5 heteroatom. The barrier to inversion rises dramatically from ammonia to phosphine to arsine as seen in Table I.<sup>9</sup> After briefly reviewing existing theories of this trend, we offer a simple molecular orbital description.

In 1947<sup>10</sup> Walsh stated the following rule: *If a group X attached to carbon is replaced by a more electronegative group Y, then the carbon valency toward Y has more p character than it had toward X.* Bent<sup>11</sup> later reformulated it as: *atomic s character concentrates in orbitals directed toward electropositive substituents.* In applying the rule to molecules of the type 1, Bent considered lone pairs as bound

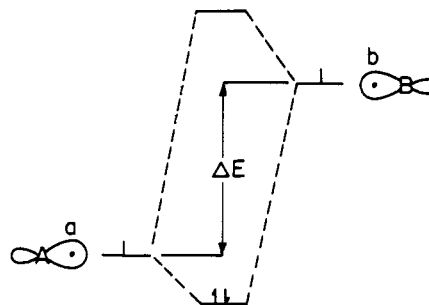


to groups of infinite electropositivity. Increasing the electronegativity of X increases the s character and lowers the energy of the lone pair. It follows that the more electronegative the substituent X, the more energetically costly will be the excursion to a transition state in which the lone pair resides in a pure p orbital.

The rule is consistent with two well-documented properties of the pyramidal inversion barrier<sup>1</sup>: (1) its increase with increasing substituent electronegativity and, of particular interest in the present study, (2) its increase with decreasing electronegativity of the inverting center (Table I). In the latter case decreasing the electronegativity of the central

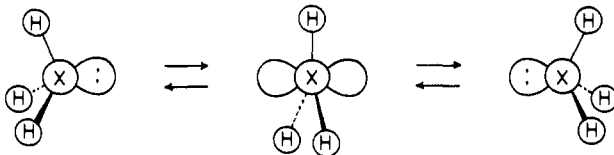
atom is equivalent to increasing the *relative* electronegativity of hydrogen, thereby reducing to a special case of (1).

The Walsh-Bent rule can be understood qualitatively using simple perturbation theory arguments.<sup>12</sup> Consider two orbitals, a and b, centered on atoms A and B, respectively. We now allow them to interact to form a bond:



Their interaction increases with (1) decreasing energy separation  $\Delta E$  and (2) increasing overlap of the two orbitals. As A becomes more electronegative, a's energy drops, its spatial distribution contracts, and its overlap with b diminishes. Reduced interaction with b is the result. In reacting to the perturbation, b tries to improve its overlap with the now more contracted orbital a. It does so by increasing its directionality, i.e., p character. The rehybridization of B which this requires must, of course, reduce the p character, hence increase the s character, of the remaining less electronegative substituents.

Murrell et al.<sup>13</sup> explain the greater lone pair s character with decreasing electronegativity in terms of differential hydrogen 1s-central atom ns and np overlap. They note that 1s-2s overlap for second row elements like nitrogen is substantially greater than 1s-2p overlap, leading to relatively large s character in the bonding orbitals at the ex-

Table I. Inversion Barriers for Group 5 Hydrides<sup>a</sup>


X	N	P	As	Sb
Electronegativity <sup>a</sup>	3.04	2.19	2.18	2.05
Barrier, <sup>b</sup> kcal/mol	5.60	27.00	34.00	29.00

<sup>a</sup> A. L. Allred and A. N. Hensley, Jr., *J. Inorg. Nucl. Chem.*, 17, 43 (1961); A. L. Allred, *ibid.*, 17, 215 (1961). <sup>b</sup> See ref 6e.

pense of the lone pair. The reduced electronegativity of third row elements like phosphorus makes 1s-3p overlap relatively more favorable with respect to 1s-3s; less s character in the bonding orbitals and more s character in the lone pair results.

We now add a third view of this trend which (a) gives a simple Walsh-type molecular orbital picture, (b) shows that it is reflected in level spacings of the corresponding united atoms, (c) relates it to the second order Jahn-Teller effect of Bader and Pearson, and (d) can be extended to include substituent effects.

### Molecular Orbital Description

The starting point of our analysis is the familiar Walsh correlation diagram for the pyramidalization of a planar  $\text{XH}_3$  molecule.<sup>14</sup> Figure 1 shows the valence molecular orbitals of  $D_{3h}$  (planar) and  $C_{3v}$  (pyramidal)  $\text{XH}_3$  which figure in the Walsh picture. Figure 2 charts, qualitatively, one-electron orbital-energy changes as a function of HXH angle  $\theta$ . Geometrically significant  $\theta$  values are  $120^\circ$  (planar),  $109.47^\circ$  (tetrahedral), and  $90^\circ$  (octahedral fragment). The  $\text{XH}_3$  MO's and their changes on pyramidalization have been discussed previously,<sup>15</sup> but, since they play a prominent role in our discussion, we briefly reexamine them here.

The lowest energy valence shell MO,  $a_{1'}$  in  $D_{3h}$ ,  $a_1$  in  $C_{3v}$ , is an in-phase combination of hydrogen 1s and X *ns* orbitals. It has no nodes and moves to lower energy with increasing pyramidalization. Perturbation theory<sup>12</sup> provides a convenient framework in which to analyze such changes, so we digress shortly to recall some familiar results.

Equation 1 is the well-known expression for the energy to second order, for a wave function,  $\phi_i^0$ , which has been subjected to a perturbation *P*:

$$\epsilon_i^{(2)} = \epsilon_i^0 + \langle \phi_i^0 | P | \phi_i^0 \rangle + \sum_{j \neq i}^{\text{all MO's}} \frac{\langle \phi_i^0 | P | \phi_j^0 \rangle^2}{\epsilon_i^0 - \epsilon_j^0} \quad (1)$$

$\epsilon_i^{(2)}$  and  $\epsilon_i^0$  are the energies of perturbed and unperturbed  $\phi_i^0$ , respectively. The second and third terms on the right-hand side of eq 1 are the first- and second-order corrections to the energy and have simple qualitative interpretations.

The second term is the perturbation averaged over the unperturbed wave functions. It corresponds in the usual Walsh argument to saying that as  $1a_{1'}$  is pyramidalized, increased overlap of the in-phase hydrogens lowers the orbital energy. Phase relationships in the *unperturbed* orbital have been used to draw conclusions about the sign of the first-order correction to the energy.

The third term in eq 1 describes a relaxation process in which electrons of a planar  $\text{XH}_3$  reorganize to minimize the energy of the new pyramidal geometry. Although the sum runs over all MO's, many of the terms will vanish. In the present case, for example, only those  $D_{3h}$  orbitals having the same  $C_{3v}$  symmetry as  $1a_{1'}$ , namely  $2a_{1'}$  and  $1a_2''$ ,

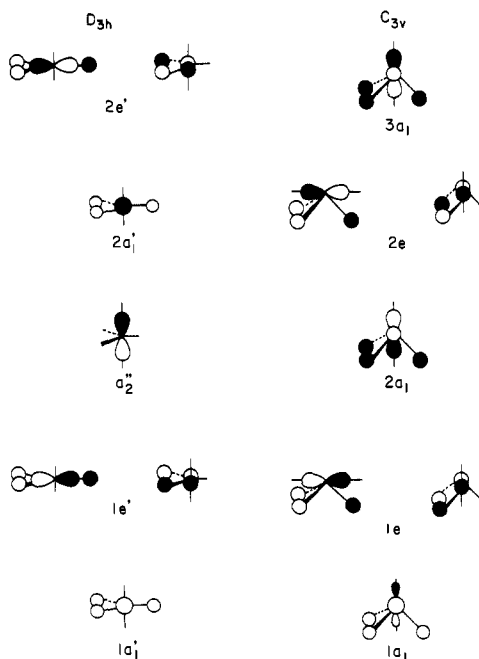


Figure 1. The valence molecular orbitals of planar ( $D_{3h}$ ) and pyramidal ( $C_{3v}$ )  $\text{XH}_3$ . Atomic orbital contributions are not to scale.

make non-zero contributions. Second-order energy corrections then arise from perturbation-induced mixture of formerly orthogonal orbitals, i.e., rehybridization. First-order corrections are usually, but not always, larger than their second-order counterparts.

Returning to Figure 1, we find the next levels above  $1a_{1'}$  to be a degenerate set,  $e'$  in  $D_{3h}$ ,  $e$  in  $C_{3v}$ , in-phase combinations of  $p_x$  and  $p_y$  orbitals on X with symmetry adapted combinations of hydrogen 1s functions. The first-order Walsh argument predicts an energy increase with out-of-plane bending as the in-phase overlap between hydrogen 1s and heavy-atom p orbitals is attenuated.

Above the  $e'$  set lies  $a_2''$ , a pure  $2p_z$  lone pair in a planar  $\text{XH}_3$ . Here there can be no first-order energy correction due to pyramidalization in a one-electron treatment. The unperturbed orbital is nonbonding with no contributions from the hydrogens; geometry changes can neither increase nor decrease bonding-antibonding phase relationships. In second order, however, both  $1a_{1'}$  and  $2a_{1'}$  mix into  $a_2''$ . It is this mixing, in particular that with  $2a_{1'}$ , which forms the basis for our analysis of central atom electronegativity effects below.

The first unfilled orbital in planar  $\text{XH}_3$  is  $2a_{1'}$ , the out-of-phase combination of *ns* on X with three in-phase hydrogen 1s orbitals. In first order, bending lowers the energy of  $2a_{1'} - 3a_1$  in  $C_{3v}$ , via increased overlap of the in-phase hydrogens. There is, however, a second-order destabilization arising from interaction with the lower lying orbitals of a symmetry. We return to this point below, simply noting here that the second-order term appears to dominate in actual calculations.

Highest lying in Figure 1 is another  $e'$  set, the antibonding counterparts of  $1e'$ . The first-order Walsh description of the energy change on bending is, as expected, the reverse of that for  $1e'$ . Reduction of antibonding overlap during pyramidalization lowers the energy. The Walsh diagram of Figure 2 provides a simple qualitative picture of the inversion barrier for eight-electron  $\text{XH}_3$  systems (e.g.,  $\text{NH}_3$ ,  $\text{PH}_3$ ,  $\text{CH}_3^-$ ,  $\text{H}_3\text{O}^+$ , etc.).  $1a_{1'}$  and  $1a_2''$  drop in energy with pyramidalization faster than the  $1e'$  set rises. A nonplanar geometry is clearly preferred.

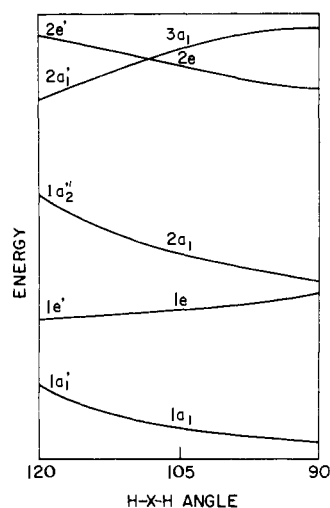
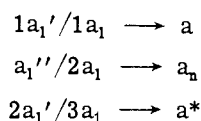


**Figure 2.** Qualitative behavior of  $XH_3$  one-electron valence-orbital energies as a function of H-X-H angle. Symmetry designations are for  $D_{3h}$  (left) and  $C_{3v}$  (center) geometries.

### Effect of Central Atom Electronegativity

The subsequent discussion deals nearly exclusively with the  $a$  levels of  $D_{3h}$  and  $C_{3v}$   $XH_3$  molecules. We now adopt a concise notation for these orbitals, for convenience making no distinction between planar and pyramidal forms:



The subscript  $n$  and superscript  $*$  are to remind the reader of the respective nonbonding and antibonding character of these orbitals.

Our analysis focuses on the LUMO,  $a^*$ , of  $XH_3$ . We argue that differential  $a^*-a_n$  mixing in the reduced  $C_{3v}$  symmetry of the pyramidal form is the single most important factor influencing the large differences in  $XH_3$  inversion barriers. That the phosphine inversion barrier is substantially larger than that for ammonia (i.e., phosphine shows the greater preference to be pyramidal) is a consequence of stronger mixing of  $a^*$  into  $a_n$  in  $PH_3$ .

We probed this qualitative argument quantitatively with extended Hückel<sup>16</sup> (EH), CNDO/2,<sup>17</sup> and STO-3G<sup>18</sup> molecular orbital calculations. In each case the wave functions and orbital energies indicated strong  $a^*$  mixing which was greater for  $PH_3$  than  $NH_3$ .

Figure 3 depicts the resulting interaction of  $a_n$  with  $a$  and  $a^*$  when the  $XH_3$  symmetry is reduced from  $D_{3h}$  to  $C_{3v}$ . Considering pairwise interactions of orbitals, it follows from simple perturbation theory that  $a$  mixes into  $a_n$  in an antibonding way, whereas  $a^*$  does so in a bonding way. The resultant  $a_n$  orbital is a superposition of the upper level in 3a and the lower one in 3b, its final appearance reflecting in part the relative contributions of  $a$  and  $a^*$ .<sup>19</sup>

Figures 4a-c give EH, CNDO/2, and STO-3G  $a_n$  wave functions for  $NH_3$  and  $PH_3$ . In each case the hydrogens and the central atom  $p$  orbital are in phase, indicating strong admixture of  $a^*$ . Moreover, the hydrogen  $1s$  and heavy-atom  $ns$  orbital coefficients are larger for  $PH_3$  than for  $NH_3$ . We interpret this as evidence for a larger contribution from  $a^*$  in phosphine than in ammonia. Note also that  $a^*$  mixing appears to increase with the quality of the calculation.

Variations in  $NH_3$  and  $PH_3$   $a$ ,  $a_n$ , and  $a^*$  one-electron orbital energies with H-X-H angle, displayed in Table II,

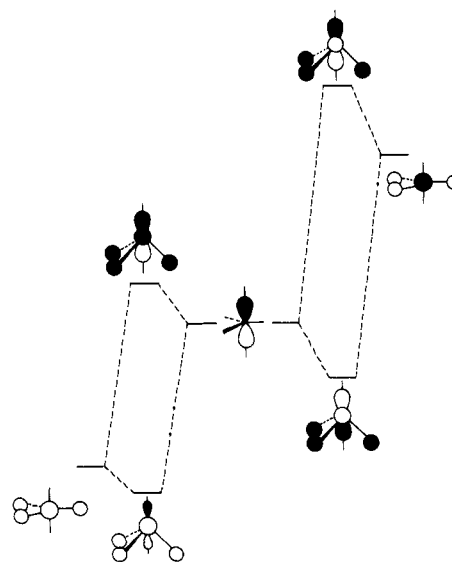


**Figure 3.** Pairwise interactions of the lone pair orbital,  $a_n$ , with a (left) and  $a^*$  (right), induced by pyramidalization of a planar  $XH_3$ . The lone pair of the pyramidal molecule will be a composite of the top orbital on the left and the bottom one on the right.

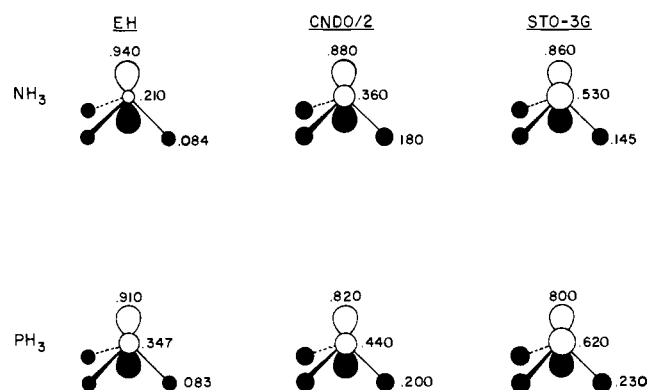


**Figure 4.** EH, CNDO/2, and STO-3G lone pair wave functions for  $NH_3$  and  $PH_3$ . Only valence atomic orbital contributions are shown. The H-X-H angle was arbitrarily chosen to be  $102^\circ$ , intermediate between the two experimental values, but close enough to the  $NH_3$  value to avoid significant H-H repulsion.

emphasize the crucial role of  $a^*$  mixing in  $XH_3$  pyramidalization. In each case both  $a$  and  $a_n$  move to lower energy. The decreasing energy of  $a$  is primarily a first-order Walsh effect, i.e., a consequence of increasing overlap between in-phase hydrogens. The corresponding energy lowering of  $a_n$ , as noted above, is a second-order phenomenon depending on the net effect of its mixings with  $a$  and  $a^*$ . That there is net stabilization of  $a_n$  as a result of these interactions is a measure of the importance of  $a^*$  mixing.

Figures 5a-c show STO-3G  $a$ ,  $a_n$ , and  $a^*$  one-electron energies as a function of HXH angle for  $NH_3$  and  $PH_3$ . The dashed line in each case is the total energy. It should be noted that while absolute energies are not to scale, relative slopes of the curves are directly comparable.

The conclusions drawn from Table II are apparent in Figure 5.  $a$  and  $a_n$  go down, while  $a^*$  goes up in energy for both  $NH_3$  and  $PH_3$ . While  $a$  drops in energy more than  $a_n$  in STO-3G ammonia, the reverse is true for phosphine. The greater sensitivity of  $a^*$  and  $a_n$  to variations in HXH angle for  $PH_3$  is noteworthy. It is the origin, we believe, of the larger  $PH_3$  inversion barrier, and may be traced to the relative energies and compositions of the  $a^*$  and  $a_n$  orbitals in the planar forms of the two molecules.

Table II. NH<sub>3</sub> and PH<sub>3</sub> Orbital and Total Energies vs. Bond Angle<sup>a,b</sup>

	EH			CNDO/2			STO-3G		
	120°	105°	90°	120°	105°	90°	120°	105°	90°
NH <sub>3</sub>									
1a <sub>1</sub> '	-27.99	-27.97	-27.95	-36.03	-37.24	-38.21	-28.32	-29.86	-31.03
1e'	-16.73	-16.41	-16.00	-20.51	-20.15	-19.23	-15.65	-15.58	-15.08
1a <sub>2</sub> ''	-13.40	-13.83	-14.24	-14.85	-16.45	-17.59	-8.45	-9.75	-11.00
2a <sub>1</sub> '	+17.45	+20.23	+21.05	+7.59	+9.07	+10.20	+16.08	+17.64	+18.35
2e'	+3.56	+2.13	+1.16	+10.52	+9.40	+8.58	+21.63	+19.76	+18.41
E <sub>total</sub>	-149.69	-149.27	-148.38	-376.95	-377.42	-376.67	-1508.46	-1508.90	-1508.31
PH <sub>3</sub>									
1a <sub>1</sub> '	-21.53	-21.57	-21.61	-25.64	-26.46	-27.17	-20.56	-21.63	-21.99
1e'	-17.66	-17.40	-17.05	-17.96	-17.52	-16.61	-12.86	-12.86	-12.18
1a <sub>2</sub> ''	-14.00	-14.49	-14.90	-10.85	-12.70	-13.83	-4.80	-5.93	-8.43
2a <sub>1</sub> '	+9.20	+17.20	+25.82	+2.86	+4.81	+4.97	+10.31	+14.37	+17.75
2e'	+4.36	+1.49	-0.93	+6.44	+5.58	+6.04	+16.65	+14.38	+12.80
E <sub>total</sub>	-141.70	-141.72	-141.24	-254.86	-256.42	-256.35	-9211.49	-9213.82	-9214.24

<sup>a</sup> Energies in eV. <sup>b</sup> Symmetry designations are for D<sub>3h</sub>.

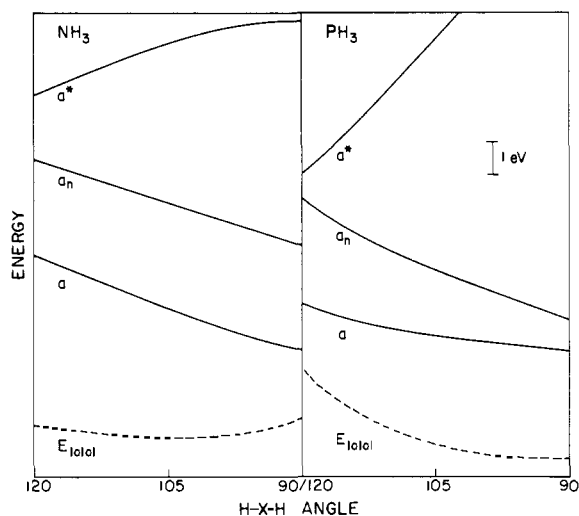


Figure 5. Dependence of STO-3G a, a<sub>n</sub>, and a\* one-electron orbital energies on the H-X-H angle for NH<sub>3</sub> and PH<sub>3</sub>. The total energy dependence (dashed line) is included for comparison. Geometrically significant angles are 120° (planar), 109.47° (tetrahedral), and 90° (pseudo-octahedral). Energy changes have been accurately reproduced; absolute energies are not to scale.

Table III. HOMO-LUMO Energy Separations

	ΔE(NH <sub>3</sub> ) <sup>a</sup>	ΔE(PH <sub>3</sub> ) <sup>a</sup>
EH	+30.85	+23.20
CNDO/2	+22.44	+12.71
STO-3G	+24.53	+15.11

<sup>a</sup> ΔE = E<sub>a\*</sub> - E<sub>a</sub>; energies in eV.

Inspection of Table II demonstrates that for each of the methods used the a\* virtual orbital lies at substantially lower energy in PH<sub>3</sub> than in NH<sub>3</sub>. Moreover, in the two SCF methods the lone pair orbital, a<sub>n</sub>, lies considerably higher in energy in phosphine than in ammonia. Both effects reduce the a<sub>n</sub>-a\* energy gap in PH<sub>3</sub> relative to NH<sub>3</sub>. Simple perturbation theory predicts that the smaller a<sub>n</sub>-a\* energy gap in PH<sub>3</sub> allows stronger interaction than for the analogous NH<sub>3</sub> pair. For all three methods the one-electron energy separation between a<sub>n</sub> and a\* is about 7-10 eV greater in NH<sub>3</sub> as shown in Table III.

We are aware of the dangers inherent in supporting a qualitative Walsh-type argument with SCF one-electron energy trends, especially for virtual orbitals.<sup>20</sup> Nevertheless, we believe the relative behavior of the a\* orbitals in am-

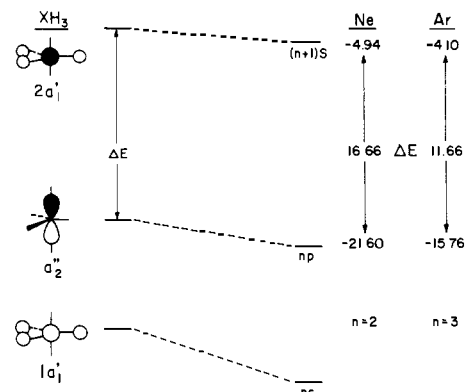


Figure 6. United atom correlation diagram for a planar XH<sub>3</sub>. Valence shell 1a<sub>1</sub>' and 2a<sub>1</sub>' molecular orbitals correlate with s atomic orbitals of the united atom, 2s and 3s in neon for ammonia, and 3s and 4s for phosphine. The 1a<sub>2</sub>'' molecular orbitals transform smoothly into 2p and 3p atomic orbitals of neon and argon, respectively. Energies are in eV.

nia and phosphine is realistic, reflecting merely the greater electronegativity of nitrogen than phosphorus. The smaller a<sub>n</sub>-a\* separation in PH<sub>3</sub> than in NH<sub>3</sub> is mirrored clearly in the np-(n + 1)s splittings in the corresponding united atoms, neon and argon. Consider the united atom correlation diagram in Figure 6. The nodal properties of the a\* orbitals in NH<sub>3</sub> and PH<sub>3</sub> require that they correlate with 3s and 4s united atom orbitals of neon and argon, respectively. In similar fashion the a<sub>n</sub> levels transform into neon 2p and argon 3p atomic orbitals. The larger splitting in neon is, of course, simply a consequence of poorer electronic screening of the nuclear charge than in argon.

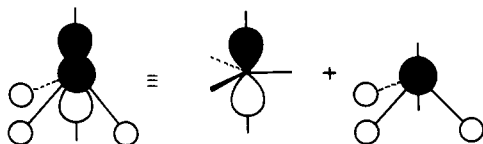
### Perturbation Theory Analysis

To examine the a<sub>n</sub>-a\* mixing in more detail we analyzed their interaction quantitatively using perturbation theory. Our method, specifically designed for use within the extended Hückel formalism, has been described previously.<sup>12,21</sup> The following discussion is therefore strictly applicable only to the EH results. Since these appear to consistently underestimate the degree of a<sub>n</sub>-a\* mixing compared to the SCF methods (see Tables II and III), we expect the results discussed below to be accentuated by similar analyses within an SCF framework.<sup>22</sup>

Figure 7 shows the results of our perturbation analysis. PH<sub>3</sub> and NH<sub>3</sub> wave functions at an arbitrary HXH angle (102°) were expanded to second order in the zero-order

wave functions of the unperturbed (planar) molecules, allowing us to compare relative extents of  $a$  and  $a^*$  mixing with  $a_n$  upon pyramidalization. The actual EH  $a_n$  wave function along with its CNDO/2 and STO-3G counterparts in Figure 4 should be considered for comparison.

The decomposition of pyramidal  $\text{NH}_3$   $a_n$  into contributions from planar  $a$ ,  $a_n$ , and  $a^*$  orbitals shows that  $a^*$  mixing (0.148) exceeds that from  $a$  (0.067) by more than a factor of 2. The predominant contributor, of course, is the pure  $2p$  lone pair orbital,  $a_n$ , of planar ammonia. Note that the dominance of  $a^*$  mixing is clearly visible in the appearance of pyramidal  $a_n$ :



The net effect of mixing is introduction into  $a_n$  of what, in its nodal properties, is essentially pure  $a^*$ .

Inspection of Table II reveals that in planar  $\text{NH}_3$ , extended Hückel  $a_n$  and  $a$  levels lie much closer in one-electron energy (14.06 eV) than  $a_n$  and  $a^*$  (30.85 eV). Recall now that the first-order correction to the wave function takes the form:<sup>23</sup>

$$a_n^{(1)} = a_n^{(0)} + C_1 a + C_2 a^* \quad (2)$$

where

$$C_1 = \langle a | P | a_n \rangle / (\epsilon_{a_n} - \epsilon_a); C_2 = \langle a^* | P | a_n \rangle / (\epsilon_{a_n} - \epsilon_{a^*}) \quad (3)$$

Clearly the energy denominator favors a larger contribution from  $a$  than  $a^*$ . The dominance of  $a^*$  mixing must therefore be determined by the relative magnitudes of the perturbation matrix elements in the numerator. In our treatment these terms are directly proportional to the corresponding overlap integrals in the pyramidal geometry:

$$\langle a | P | a_n \rangle = k \langle a | a_n \rangle \quad (4)$$

$$\langle a^* | P | a_n \rangle = k \langle a^* | a_n \rangle \quad (5)$$

The relative contributions of  $a^*$  and  $a$  to  $a_n^{(1)}$  are given by the coefficient ratio:

$$\frac{C_2}{C_1} = \frac{\langle a^* | P | a_n \rangle}{\langle a | P | a_n \rangle} \left( \frac{\epsilon_{a_n} - \epsilon_a}{\epsilon_{a_n} - \epsilon_{a^*}} \right) = \frac{\langle a^* | a_n \rangle}{\langle a | a_n \rangle} \left( \frac{\epsilon_{a_n} - \epsilon_a}{\epsilon_{a_n} - \epsilon_{a^*}} \right) \quad (6)$$

For an HNH angle of  $102^\circ$  the values of  $\langle a^* | a_n \rangle$  and  $\langle a | a_n \rangle$  are 0.4254 and 0.0910, respectively. It follows that:

$$\frac{C_2}{C_1} = \left( \frac{0.4254}{0.0910} \right) \left( \frac{14.06}{30.85} \right) = 2.1 \quad (7)$$

The overlap term, favoring  $a^*$  mixing, is seen to dominate the energy denominator term which favors  $a$ .

The large overlap of  $a_n$  with  $a^*$ , nearly fivefold greater than with  $a$ , is a consequence of the nodal properties of the  $a_n$  and  $a^*$  orbitals. Whereas  $a$ , neglecting inner shells, has no nodes,  $a_n$  and  $a^*$  each have one node; the closeness of their local symmetry is reflected in a larger overlap.

The nodal properties enter the overlap calculation in a subtle way. The antibonding character of the  $a^*$  orbital, with its attendant negative overlap between hydrogens and heavy atom, manifests itself, via normalization, in large coefficients on both hydrogen and heavy-atom orbitals. The EH wave functions for  $a$  and  $a^*$  demonstrate this dramatically:

$$a = 0.1548(H_{1s} + H_{1s} + H_{1s}) + 0.7532(N_{2s})$$

$$a^* = 0.7235(H_{1s} + H_{1s} + H_{1s}) - 1.2597(N_{2s})$$

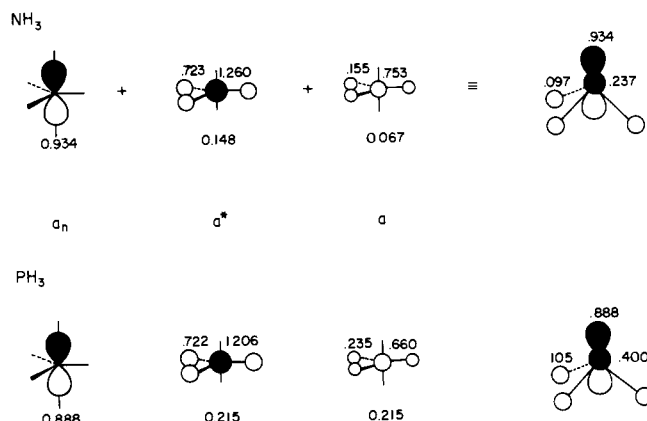


Figure 7. Expansion of EH lone pair molecular orbitals for  $\text{NH}_3$  and  $\text{PH}_3$  to second order (right) in terms of wave functions of the unperturbed (planar)  $\text{XH}_3$  antecedents (left). Numbers above the structures are valence atomic orbital coefficients, those below are contributions of the unperturbed molecular orbitals to the second-order wave function. The H-X-H angle was arbitrarily chosen to be  $102^\circ$  (see Figure 4 caption).

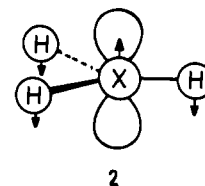
The large hydrogen  $1s$  orbital coefficients are ultimately responsible for the much larger value of  $\langle a^* | a_n \rangle$  than  $\langle a | a_n \rangle$ .

An analogous decomposition of the extended Hückel  $\text{PH}_3$  lone pair is given in Figure 7 (bottom). Both  $a$  and  $a^*$  make larger contributions than in  $\text{NH}_3$ , a consequence of their closer proximity to  $a_n$  when nitrogen is replaced by less electronegative phosphorus. Equal contributions from  $a$  and  $a^*$  are obtained, but  $a^*$  prevails in the final wave function because of its larger coefficients on hydrogen.

In a qualitative way, then, we may regard  $a_n$  as a composite of  $np$  of X and that part of the dominant  $a^*$  contribution remaining after the "opposing" a contribution has been superimposed. Reexamination of Figure 4 emphasizes that this result is independent of the level of approximation of the calculation.

A final consideration regarding the importance of  $a^*$  mixing derives from the second order Jahn-Teller effect of Bader, stereochemical consequences of which have been explored recently by Pearson.<sup>24</sup> A molecule will undergo second-order Jahn-Teller geometrical distortion, if there is vibronic coupling of a "low-lying" electronic excited state with a normal vibrational mode of the same symmetry. The geometrical distortion lowers the molecular symmetry and is controlled by the nature of the normal mode doing the coupling.

The lowest lying excited state in a planar  $\text{NH}_3$  or  $\text{PH}_3$  in our calculations<sup>25</sup> arises via promotion of an electron from  $a$  to  $a^*$ . The transition, of symmetry  $a_2'' \times a' = a_2''$ , is electronically allowed and polarized along the molecular threefold axis. The normal mode with which it couples, also of  $a_2''$  symmetry, is shown in 2. As noted by Pearson, it is just the one necessary to pyramidalize a planar  $\text{XH}_3$ .



### Substituent Effects

We have so far only considered factors affecting inversion barriers in the parent compounds. Substitution produces marked changes in the barrier height. The effects are well understood and have been discussed in detail by oth-

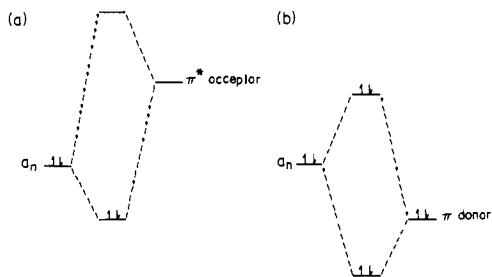
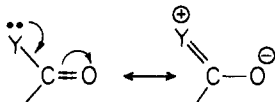


**Figure 8.** Qualitative interaction diagrams for a lone pair with (a) a  $\pi$  acceptor (net stabilization) and (b) a  $\pi$  donor (net destabilization with inclusion of overlap).

ers.<sup>1,5b-d</sup> The following generalization can be made: substituents donating electrons by resonance ( $\pi$  donors) or withdrawing them by induction ( $\sigma$  acceptors) raise the barrier; those withdrawing electrons by resonance ( $\pi$  acceptors) or relaxing them inductively lower it. We conclude the present study with a molecular orbital picture of these effects which incorporates the role of  $a^*$  mixing.

For our purposes substituent effects are grouped into two classes:  $\sigma$  and  $\pi$ . We consider first  $\pi$  effects. Figure 8 shows typical two-orbital interaction diagrams for a lone pair with: (a) a  $\pi$  acceptor and (b) a  $\pi$  donor. In each case the lower level is stabilized, the upper one destabilized (with inclusion of overlap its destabilization is greater than the stabilization of the lower level).

For the  $\pi$  acceptor of Figure 8a the upper level is unoccupied. The two lone pair electrons enter the lower level with concomitant decrease in energy. This is, of course, nothing more than a molecular orbital description of resonance stabilization:



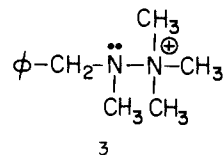
The magnitude of the stabilization depends in the usual way on the energy separation of the two interacting groups. Lone pair overlap with an adjacent  $\pi$  substituent will be maximal when the lone pair is a pure p orbital, i.e., when nitrogen or phosphorus is planar. It follows that  $\pi$  acceptors favor planar over pyramidal geometry and therefore reduce the barrier to inversion.

The situation is exactly reversed for the  $\pi$  donor of Figure 8b where the upper level is now filled. The interaction, net destabilizing, will again be maximal for a planar nitrogen or phosphorus. Accordingly,  $\pi$  donors raise the inversion barrier.

$\sigma$  substituent effects<sup>26</sup> enter our analysis by influencing the extent of  $a_n$ - $a^*$  mixing. A substituent which increases this mixing relative to the unsubstituted molecule favors pyramidalization and raises the inversion barrier; similarly, one which decreases it also lowers the barrier.

Electronegative  $\sigma$  substituents lower all levels of an  $\text{XH}_3$  derivative with respect to the parent molecule. CNDO/2 calculations on a planar  $\text{NH}_3$ , in which the H atom coulomb integrals have been systematically made more negative to simulate the effect of electronegative  $\sigma$  substituents,<sup>27</sup> bear this out.  $a_n$ , which has zero overlap with the hydrogens in the planar geometry, nevertheless shifts to lower energy, a consequence of the reduced charge on nitrogen. As might have been anticipated, it shifts to a lesser degree than those levels having nonzero coefficients on the electronegative hydrogen atoms. The  $a_n$ - $a^*$  energy gap decreases with increasing electronegativity of the substituents;  $\sigma$ -electron withdrawers increase the barrier. An analogous argument for  $\sigma$  donors predicts that they should lower the barrier.

A recurring difficulty in analyzing substituent effects has been disentangling  $\sigma$  and  $\pi$  effects. For electronegative lone-pair-bearing substituents like  $\text{NR}_2$ , OR, and halogen,  $\sigma$ -acceptors but  $\pi$  donors, the effects are symbiotic. Both increase the inversion barrier; assessing their relative contributions experimentally is not an easy task. Griffith and Roberts,<sup>28</sup> for example, have tried to isolate the  $\sigma$ -acceptor effect by studying the influence of the electron-withdrawing quaternary ammonium group in **3**. They find an unusually small inversion barrier, but point out that the result is equivocal owing to a likely steric effect which preferentially destabilizes the pyramidal conformer.



**3**

We resist here the temptation to quantitatively partition substitution into  $\sigma$  and  $\pi$  effects. It is clear from the present study that  $\sigma$ -electronegativity effects exert a significant effect on the inversion barrier. A particularly interesting illustration is found in recent ab initio calculations by Csizmadia et al. on aminophosphine.<sup>29</sup> The  $\text{NH}_2$  group is calculated to be planar, whereas the phosphorus is pyramidal with an inversion barrier (42.6 kcal/mol) considerably larger than that for phosphine. Substitution of  $\text{NH}_2$  for H in  $\text{PH}_3$  introduces a more electronegative group, whereas the analogous replacement of H with  $\text{PH}_2$  in  $\text{NH}_2$  actually introduces a slightly more electropositive group.<sup>30</sup> On balance, our experience with  $\pi$ -donor and  $\pi$ -acceptor substituent effects on inversion barriers<sup>31</sup> leaves us in agreement with others<sup>1,5b</sup> who have concluded that  $\pi$  effects significantly outweigh  $\sigma$  effects. On the other hand, it is clear from the present work that the latter are not negligible, making an important, if not dominant, contribution to the inversion barriers of  $\text{XH}_3$  derivatives.

The extent to which substituent or central atom d orbitals influence inversion barrier magnitudes has been a persistent consideration in previous discussions. Our position has been to avoid invoking them, believing as others have<sup>1c,3b,29a,32</sup> that their participation, where demonstrable, has mathematical rather than chemical significance. We have found the various characteristics of the barrier to be reproducible without recourse to d orbitals. Where they have been included in the basis set, they have modified rather than reversed trends, thus influencing the barrier quantitatively, but not qualitatively. Practically speaking, including d orbitals introduces five relatively low-lying acceptor orbitals capable of interacting with the four filled valence orbitals of an eight-electron  $\text{XH}_3$  system. One of these,  $d_{z^2}$ , has the proper symmetry to interact with  $a_n$  and thus functions as a surrogate  $a^*$  in the pyramidalization process. Since such an orbital lies substantially closer in energy to  $a_n$  than  $a^*$ , its mixing with  $a_n$  is greater and so too is the preference for nonplanarity which this mixing induces. Since d orbital participation is, of course, more likely for phosphorus than nitrogen, it should and does accentuate the already greater preference of  $\text{PH}_3$  over  $\text{NH}_3$  to be pyramidal.<sup>33,34</sup>

**Acknowledgment.** The author wishes to thank P. J. Hay, P. Hofmann, and J. Thibeault for a number of helpful discussions. Special gratitude is expressed to R. Hoffmann for his hospitality and interest in this work during a visit to Cornell. Acknowledgment is also made to the donors of The Petroleum Research Fund, administered by the American Chemical Society, for the support of this research.

## References and Notes

- (1) For recent reviews see: (a) S. J. Brois, *Ann. N.Y. Acad. Sci.*, **31**, 931 (1969); (b) H. Kessler, *Angew. Chem.*, **82**, 237 (1970); (c) A. Rauk, L. C. Allen, and K. Mislow, *ibid.*, **453** (1970); (d) J. M. Lehn, *Fortschr. Chem. Forsch.*, **15**, 311 (1970); (e) J. B. Lambert, *Top. Stereochem.*, **6**, 19 (1971).
- (2) Recent ab initio calculations on  $\text{NH}_3$  include: (a) A. Pipano, R. R. Gilman, C. F. Bender, and I. Shavitt, *Chem. Phys. Lett.*, **4**, 583 (1970); (b) A. Rauk, L. C. Allen, and E. Clementi, *J. Chem. Phys.*, **52**, 4133 (1970), and references therein.
- (3) Recent ab initio calculations on  $\text{PH}_3$  include: (a) D. B. Boyd and W. N. Lipscomb, *J. Chem. Phys.*, **46**, 910 (1967); (b) J. M. Lehn and B. Munsch, *Chem. Commun.*, 1327 (1969); (c) I. H. Hillier and V. R. Saunders, *ibid.*, 316 (1970); (d) A. Rauk, L. C. Allen, and K. Mislow, *J. Am. Chem. Soc.*, **94**, 3035 (1972).
- (4) For SCF-CI calculations on  $\text{CH}_3$  and  $\text{CF}_3$  see: K. Morokuma, L. Pedersen, and M. Karplus, *J. Chem. Phys.*, **48**, 4801 (1968).
- (5) Leading references to semiempirical calculations of inversion barriers are: (a) M. J. S. Dewar and M. Shanshal, *J. Am. Chem. Soc.*, **91**, 3654 (1969); (b) K. Müller, *Helv. Chim. Acta*, **53**, 1112 (1970); (c) A. Rauk, J. D. Andose, W. G. Frick, R. Tang, and K. Mislow, *ibid.*, **93**, 6507 (1971); (d) J. D. Andose, A. Rauk, and K. Mislow, *ibid.*, **96**, 6904 (1974).
- (6) For work on pyramidal inversion barriers from the viewpoint of vibrational spectroscopy see: (a) J. F. Kincaid and F. C. Henriques, Jr., *J. Am. Chem. Soc.*, **62**, 1474 (1940); (b) C. C. Costain and G. B. M. Sutherland, *J. Phys. Chem.*, **56**, 321 (1952); (c) R. E. Weston, Jr., *J. Am. Chem. Soc.*, **76**, 2645 (1954); (d) R. S. Berry, *J. Chem. Phys.*, **32**, 933 (1960); (e) G. W. Koepl, D. S. Sagatys, G. S. Krishnamurthy, and S. I. Miller, *J. Am. Chem. Soc.*, **89**, 3396 (1967); (f) G. Herzberg, "Molecular Spectra and Molecular Structure. II. Infrared and Raman Spectra of Polyatomic Molecules", Van Nostrand, Princeton, N.J., 1945, p 295 ff.
- (7) J. D. Swalen and J. A. Ibers, *J. Chem. Phys.*, **36**, 1914 (1962).
- (8) D. M. Dennison and G. E. Uhlenbeck, *Phys. Rev.*, **41**, 313 (1932).
- (9) (a) Experimental barriers for the group 5 hydrides, with the exception of ammonia, are not available. The results in Table I were calculated by Koepl et al.<sup>6e</sup> using the Costain-Sutherland harmonic valence force field  $V = K(\Delta\alpha)^2$ , where  $K$  is a constant for each molecule, obtained from its vibrational stretching and bending frequencies, and  $\Delta\alpha$  is the deviation of the HXH bond angle from a planar ( $120^\circ$ ) one. The force field adequately describes ammonia inversion; its application to other molecules is probably not quantitatively reliable. Koepl et al. satisfy themselves with obtaining reasonable trends in the barrier, and it is the trend in Table I which is of interest to us here. Extensive tabulations of experimental barriers of amine, phosphine, and arsine derivatives can be found in ref 1d,e and 5c,d. (b) A referee has pointed out an analogous trend in  $\text{XH}_3$  radicals of group 4 hydrides in a xenon matrix.  $\text{CH}_3$  is planar; the Si, Ge, and Sn derivatives are pyramidal. See G. S. Jackel and W. Gordy, *Phys. Rev.*, **176**, 443 (1968).
- (10) A. D. Walsh, *Discuss. Faraday Soc.*, **2**, 18 (1947); see also A. D. Walsh, *Trans. Faraday Soc.*, **42**, 56 (1946), *ibid.*, **43**, 60; 158 (1947); A. D. Walsh, *Proc. R. Soc. London, Ser. A*, **207**, 13 (1951).
- (11) H. A. Bent, *Chem. Rev.*, **61**, 275 (1961).
- (12) See, for example, L. Libit and R. Hoffmann, *J. Am. Chem. Soc.*, **96**, 1370 (1974), and references therein.
- (13) J. N. Murrell, S. F. Kettle, and J. M. Tedder, "Valence Theory", 2nd ed, Wiley, New York, N.Y., 1970, p 59.
- (14) A. D. Walsh, *J. Chem. Soc.*, 2296 (1953); G. Herzberg, "Molecular Spectra and Molecular Structure. III. Electronic Structure of Polyatomic Molecules", Van Nostrand, Princeton, N. J., 1966, pp. 318-321.
- (15) A lucid treatment has been given by B. M. Gimarc, *J. Am. Chem. Soc.*, **93**, 593 (1971); see also B. M. Deb, *ibid.*, **96**, 2030 (1974).
- (16) R. Hoffmann, *J. Chem. Phys.*, **39**, 1397 (1963); R. Hoffmann and W. N. Lipscomb, *ibid.*, **36**, 2179 (1962); **37**, 2872 (1962). Slater orbital exponents were 1.3 (H), 1.6 (P), 1.95 (N);  $H_i$  were -13.6 (H, 1 s), -26.0 (N, 2 s), -13.4 (N, 2 p), -18.6 (P, 3 s), -14.0 (P, 3 p). N-H and P-H distances were 1.10 and 1.40 Å, respectively. Extended Hückel calculations with this parametrization actually predict ammonia and phosphine to be planar, thus necessitating the SCF calculations. The  $\text{XH}_3$  preference for planarity in EH calculations can be traced to the  $1e'/1e$  levels in Figure 2, which rise too steeply with increasing pyramidality. The SCF calculations show (Table II) the energy change of the  $1e$  levels to be small compared to corresponding changes in the  $a$  levels. We report the EH results despite this failure, because their qualitative behavior properly mimics that of the SCF levels.  $1a_1'$ ,  $1a_2''$ , and  $2e'$  one-electron energies go down and  $1e'$  and  $2a_1'$  go up with increasing pyramidality. Since we focus exclusively on the  $a$  levels in the sequel, the exaggerated response of the EH  $1e'$  levels to out-of-plane bending does not affect our analysis.
- (17) J. A. Pople, D. P. Santry, and G. A. Segal, *J. Chem. Phys.*, **43**, S129 (1965); J. A. Pople and D. L. Beveridge, "Approximate Molecular Orbital Theory", McGraw-Hill, New York, N.Y., 1970. We minimized the effect of  $d$  orbitals in our calculations on  $\text{PH}_3$  by setting the  $3d$  coulomb integral equal to +1000.
- (18) W. J. Hehre, R. F. Stewart, and J. A. Pople, *J. Chem. Phys.*, **51**, 2657 (1969); J. A. Pople, *Acc. Chem. Res.*, **3**, 217 (1970). See these references for STO-3G exponents.
- (19) It should be noted, of course, that owing to its antibonding character,  $a^*$  will have larger coefficients on both hydrogens and heavy atom than its bonding counterpart. Accordingly, it is possible for  $a^*$  to make a smaller relative contribution to  $a_i$ , yet still dominate its appearance. See below.
- (20) For a critical review see: R. J. Buenker and S. D. Peyerimhoff, *Chem. Rev.*, **74**, 127 (1974), and references therein.
- (21) A. Imamura, *Mol. Phys.*, **15**, 225 (1968).
- (22) J. A. Pople, *Proc. R. Soc. London, Ser. A*, **233**, 233 (1955); R. Lefebvre and C. Moser, "Calcul des fonctions d'onde moléculaire", Editions CNRS, Paris, 1958, p 109; A. T. Amos and J. I. Musher, *Mol. Phys.*, **13**, 509 (1967); R. Sustmann and G. Binsch, *ibid.*, **20**, 1, 9 (1971).
- (23) We have simplified the usual sum to include only those mixings allowed by symmetry. The terms are those defined in connection with eq 1.
- (24) (a) R. F. W. Bader, *Can. J. Chem.*, **40**, 1164 (1962); (b) L. Salem and J. S. Wright, *J. Am. Chem. Soc.*, **91**, 5947 (1969); (c) R. G. Pearson, *ibid.*, **91**, 1252; 4947 (1969); (d) R. G. Pearson, *J. Chem. Phys.*, **52**, 2167 (1970); (e) R. G. Pearson, *Acc. Chem. Res.*, **4**, 152 (1971); (f) L. S. Bartell, *J. Chem. Educ.*, **45**, 754 (1968).
- (25) See also ref 3a,d.
- (26)  $\sigma$  substituent effects on phosphine and arsine inversion barriers have been investigated extensively by Mislow and coworkers: R. D. Baechler and K. Mislow, *J. Am. Chem. Soc.*, **92**, 4758 (1970); *ibid.*, **93**, 773 (1971); R. H. Bowman and K. Mislow, *ibid.*, **94**, 2859 (1972), and references therein.
- (27) A similar strategy has been employed in ab initio calculations to simulate electronegative substituents using hydrogen, by increasing its nuclear charge. See, for example, ref 1c, p 402; P. Kollman, *J. Am. Chem. Soc.*, **96**, 4363 (1974).
- (28) D. L. Griffith and J. D. Roberts, *J. Am. Chem. Soc.*, **87**, 4089 (1965).
- (29) (a) I. G. Csizmadia, A. H. Cowley, M. W. Taylor, L. M. Tel, and S. Wolfe, *Chem. Commun.*, 1147 (1972); (b) I. G. Csizmadia, A. H. Cowley, M. W. Taylor, and S. Wolfe, *Chem. Commun.*, 432 (1974); (c) see also, A. H. Cowley, M. J. S. Dewar, W. R. Jackson, and W. B. Jennings, *J. Am. Chem. Soc.*, **92**, 5206 (1970).
- (30) The electronegativity of H (2.20) is slightly greater than that of trivalent phosphorus (2.19): A. L. Allred and A. N. Hensley Jr., *J. Inorg. Nucl. Chem.*, **17**, 43 (1961); A. L. Allred, *ibid.*, **17**, 215 (1961).
- (31) C. C. Levin, unpublished data.
- (32) (a) R. S. Mulliken, *J. Chem. Phys.*, **36**, 3428 (1962); (b) C. A. Coulson, *Nature (London)*, **221**, 1106 (1969).
- (33) For an HPH angle of  $90^\circ$ , our CNDO/2 calculations on  $\text{PH}_3$  which included  $d$  orbitals gave an inversion barrier of 64.0 kcal/mol as compared with 34.4 kcal/mol without them.
- (34) NOTE ADDED IN PROOF: N. Epiotis and W. Cherry, *J. Am. Chem. Soc.*, in press, have given a similar interpretation of the trend in  $\text{XH}_3$  inversion barriers in an independent study. We thank Professor Epiotis for making a copy of the manuscript available prior to publication.